HSL

Volume 14

Number 22

November 4, 1975

Biochemistry
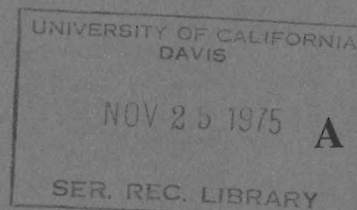
A biweekly

publication

of the

American Chemical

Society

L-Phenylalanine:tRNA Ligase of *Escherichia coli* K10. A Rapid Kinetic Investigation of the Catalytic Reaction[†]

Peter Bartmann, Till Hanke, and Eggehard Holler*

ABSTRACT: The kinetics of the amino acid activation and the transfer of the amino acid to tRNA have been investigated for L-phenylalanine:tRNA ligase of *Escherichia coli* K10 by stopped-flow and radioactive techniques. The rapid kinetics were followed by the observation of the displacement of the fluorescent dye, 6-*p*-toluidinylnaphthalene-2-sulfonate from the binding site of L-phenylalanine under conditions where a single active site of the enzyme was involved. The following results are of particular interest. (1) Equilibrium binding of L-phenylalanine and tRNA^{Phe} indicates in each case two sites of interaction with an approximately tenfold difference of the binding affinity. (2) Experimental conditions of the kinetic investigation were chosen to favor reactions at the high affinity binding sites. Under those conditions, the rate constants have been evaluated at 1 mM magnesium to be in the range 12–25 sec^{-1} for the activation reaction and 42–77 sec^{-1} for the reverse, the variation of the values depending on those of the dissociation constants used for computation. The rate constant for the transfer reaction is 0.05 sec^{-1} and for the reverse 0.19 sec^{-1}. The forward reaction is rate limiting for the overall reaction at single turnover and steady-state conditions. (3) All rate constants depend on the concentration of magnesium. Evidence is provided that the transfer occurs via a productive enzyme–tRNA^{Phe} complex which is in a magnesium-dependent equilibrium with an unproductive complex, high magnesium favoring the former. The position of the tRNA-CCA end in the productive complex is such, that the fluorescent dye can be displaced by Phe-tRNA^{Phe}. The thermodynamics of the overall reaction have been treated on the basis of the partial reactions. The free enthalpy of the completed reaction was calculated to be very close to zero. The significance of the adenylate intermediate is discussed with respect to the product inhibition expected on the basis of the tendency of tRNA^{Phe} and L-phenylalanine to form tight complexes with the enzyme.

Previous investigations have provided considerable evidence that the aminoacylation of tRNA as catalyzed by L-amino acid:tRNA ligases proceeds via an activation of the amino acid and a subsequent transfer of this moiety to tRNA (Kisselev and Favorova, 1974, and references therein). Despite many efforts to establish the kinetics of these enzymes, none of them has been investigated beyond the time limits of the classical radioactive techniques as there are the ATP–[^{32}P]PP$_i$ exchange and ^{14}C amino acid labeling, to provide a detailed knowledge of the overall kinetics at conditions which are optimal for catalysis. In the present work we have attempted to resolve the catalytic steps, in particular those of the transfer reaction by means of stopped-flow experiments. We have also made classical radioactive measurements under single turnover and steady-state conditions. However, we have not been following the kinetics of substrate binding. In connection with previous

results we have drawn conclusions about the catalysis by L-phenylalanine:tRNA ligase (*Escherichia coli*) which may be also valid for amino acid:tRNA ligases in general.

Materials and Methods

L-Phenylalanine:tRNA ligase (specific activity 53,600 nmol mg^{-1} hr^{-1}) was prepared from *E. coli* K10 in the presence of phenylmethanesulfonyl fluoride as described by Hanke et al. (1974). Unfractionated tRNA was obtained according to Zubay (1962) from *E. coli* K10. Chromatography on benzoylated DEAE-cellulose (Gillam et al., 1967) and RPC-5 columns (Pearson et al., 1971) was applied to obtain tRNA^{Phe} having an amino acid acceptance of 1250 pmol/A_{260} unit (measured at pH 7 in H$_2$O). Enzyme activity and tRNA charging capacity were determined as described by Kosakowski and Böck (1970). Protein concentrations were measured according to Lowry et al. (1961) and Waddell (1965).

[^{14}C]Phe-tRNA^{Phe} was prepared as described previously (Bartmann et al., 1974). Uniformly labeled L-[^{14}C]phenylalanine with a specific radioactivity of 450 Ci/mol was ob-

Sipos, T., and Merkel, J. R. (1970), *Biochemistry 9*, 2766.

Smith, R. L., and Shaw, E. (1969), *J. Biol. Chem. 244*, 4704.

Solomon, I. (1955), *Phys. Rev. 99*, 559.

Stroud, R. M., Kay, L. M., and Dickerson, R. E. (1971), *Cold Springs Harbor Symp. Quant. Biol. 36*, 125.

Stroud, R. M., Kay, L. M., and Dickerson, R. E. (1974), *J. Mol. Biol. 83*, 185.

Titani, K., Ericsson, L. H., Neurath, H., and Walsh, K. A. (1975), *Biochemistry 14*, 1358.

Trowbridge, C. G., Krehbiel, A., and Laskowski, M. (1963), *Biochemistry 2*, 843.

Valenzuela, P., and Bender, M. L. (1969), *Proc. Natl. Acad. Sci. U.S.A. 63*, 1214.

Valenzuela, P., and Bender, M. L. (1970), *Biochemistry 9*, 2440.

Van Geet, A. L., and Hume, D. N. (1965), *Anal. Chem. 37*, 979.

Villanueva, G. B., and Herskovits, T. T. (1971), *Biochemistry 10*, 4589.

Walsh, K., and Neurath, H. (1964), *Proc. Natl. Acad. Sci. U.S.A. 52*, 884.

Yguerabide, J., Epstein, H. F., and Stryer, L. (1970), *J. Mol. Biol. 51*, 573.

The Molecular Structure of a Dimer Composed of the Variable Portions of the Bence-Jones Protein REI Refined at 2.0-Å Resolution[†]

Otto Epp,* Eaton E. Lattman,‡ Marianne Schiffer,§ Robert Huber, and Walter Palm#

ABSTRACT: The structure of the variable portions of a κ-type Bence-Jones protein REI forming a dimer has been determined by X-ray diffraction to a resolution of 2.0 Å. The structure has been refined using a constrained crystallographic refinement procedure. The final R value is 0.24 for 15,000 significantly measured reflections; the estimated standard deviation of atomic positions is 0.09 Å. A more objective assessment of the error in the atomic positions is possible by comparing the two independently refined monomers. The mean deviation of main-chain atoms of the two chains in internal segments is 0.22 Å, of main-chain dihedral angles 6.3° for these segments. The unrefined molecular structure of the V_{REI} dimer has been published (Epp, O., Colman, P., Fehlhammer, H., Bode, W., Schiffer, M., Huber, R., and Palm, W. (1974), *Eur. J. Biochem. 45*, 513). Now a detailed analysis is presented in terms of hydrogen bonds and conformational angles. Secondary struc-tural elements (antiparallel β structure, reverse turns) are defined. A more precise atomic arrangement of the amino acid residues forming the contact region and the hapten binding site is given as well as the localization of solvent molecules. Two *cis*-prolines (Pro-8 and Pro-95) were detected. The intrachain disulfide bridge (Cys-23–Cys-88) occurs statistically in two alternative conformations. The structure suggests reasons for strong conservation of several amino acid residues. The knowledge of the refined molecular structure enables crystal structure analyses of related molecules to be made by Patterson search techniques. The calculated phases based on the refined structure are much improved compared to isomorphous phases. Therefore the effects of hapten binding on the molecular structure can be analyzed by the difference Fourier technique with more reliability. Hapten binding studies have been started.

Immunoglobulins are proteins with specific antibody activity. There exist several classes. The IgG class of immunoglobulins is composed of two light and two heavy chains. The Bence-Jones proteins excreted by patients with multiple myeloma into the urine have been shown to be free light chains. The Bence-Jones protein REI is a human immunoglobulin light chain of κ type. The purification, crystalliza-tion, and sequence analysis has been described (Palm, 1970; Palm and Hilschmann, 1973, 1975; Palm, 1974). The crystal structure of a dimer composed of the variable portions of this Bence-Jones protein at a resolution of 2.8 Å was reported (Epp et al., 1974). Data to a resolution of 2.0 Å have now been collected and the structure has been refined by constrained crystallographic refinement. The aim was to get a detailed insight into the conformation of this molecule (main chain, side chains, and bound solvent) and to obtain a model sufficiently accurate for its use in Patterson search techniques to determine the crystal structures of related molecules (Fehlhammer et al., 1975). As refined phases are considerably better than isomorphous phases (Watenpaugh et al., 1973; Deisenhofer and Steigemann, 1975; Huber et al., 1974), the quality of difference Fourier maps will be much improved; this will make it possible to determine the structure bound haptens and the subtle structural changes which might occur upon binding.

Table I: Options and Specifications of Various Programs.

(1) Model Building (Diamond, 1966)

Probe	Probe Length	Filter Constants C_1		C_2		Variation of Dihedral Angles
1	1 0^a	0.5	1.0^a	10^{-4}	10^{-2}^{d}	ϕ,ψ,χ
2	1 2	0.5	0.5	10^{-4}	10^{-4}	ϕ,ψ,χ,τ
3	2 5	0.1	0.1	10^{-4}	10^{-4}	ϕ,ψ,χ,τ
4	5 6	0.1	0.0	10^{-4}	10^{-2}	ϕ,ψ,χ,τ
5	6 6	0.0	0.0	10^{-4}	10^{-2}	ϕ,ψ,χ,τ

Eigenshifts are permitted if either $\lambda \geqslant C_1 e^2$ or $\lambda \geqslant C_2\lambda_{max}$, where λ are eigenvalues of the normal matrix. e^2 is the residual. Variation of the folds of prolines χ^5 of arginine, and ω was not permitted. The angular value of τ (N–C$_\alpha$–C) was fixed to a value of 109.65° including model-building procedure 7. In model-building 7 cis-prolines were introduced (Huber and Steigemann, 1974). ϕ,ψ are main-chain dihedral angles, χ are side-chain dihedral angles. The angular values of main chain and side chains were used and included wherever they were known, even if only crudely.

(2) Real-Space Refinement (Diamond, 1971, 1974)

Zone length	7
Margin width	6; 8^b
Fixed radius of all atoms (Å)	1.55; 1.50^c
Relative weights of C:N:O:S	6:7:8:16
Relative softness of dihedral angles	
ψ,ϕ,χ^1–χ^4	100
χ^5	1
$\theta^1,\theta^2,\theta^3$ (proline)	0.1
θ^1,θ^2 (cysteine)	0
τ (N–C$_\alpha$–C)	0.1
ω (torsion angle $C_{i-1}{}^\alpha$–C_{i-1}–N_i–$C_i{}^\alpha$)	0.1^d

Refinement of Scale Factor (K) and Background Level (d) Only

Filter ratio $\lambda_{min}/\lambda_{max}$ for K, d refinement	0.01
Filter ratio for rotational refinement $\lambda_{min}/\lambda_{max}$	
Isomorphous map	0.005
from difference Fourier map 2 on	0.0005
from difference Fourier map 4 on	0.00007
from difference Fourier map 6 on	0.00004
The value of 0.00004 resulted in a proportion of shifts applied of about	70%
Filter ratio for translational refinement $\lambda_{min}/\lambda_{max}$	0.01
The value of 0.01 resulted in a proportion of shifts applied of about	100%

(3) Structure–Factor Calculation

(W. Steigemann and T. A. Jones) atomic scattering factors: Forsyth and Wells constants (1959), an overall temperature factor was used throughout.

(4) R Value Calculation

R is defined as

$$R = \frac{\Sigma\|F_O| - |F_C\|}{\Sigma|F_O|}$$

$|F_O|$, observed structure–factor amplitude
$|F_C|$, calculated structure–factor amplitude
For this calculation, as well as for the Fourier calculations, reflections of extremely bad correlation were excluded. The condition for exclusion was:

$$\frac{2\|F_O| - |F_C\|}{\|F_O| + |F_C\|} > 1.2$$

About 250 reflections were excluded. The innermost reflections to 6.8-Å resolution were omitted from all calculations (941).

(5) Fourier Synthesis

Grid: 1.1 Å × 1.1 Å × 1.0 Å at the beginning to a resolution of 2.4 Å, later 0.8 Å × 0.8 Å × 0.8 Å. During the course of the refinement the Fourier coefficients were mostly of the type $(2|F_O| - |F_C|)$ expα_C. Also some Fourier syntheses with coefficients $(3|F_O| - 2|F_C|)$ expα_C were used. Difference Fourier maps were calculated with coefficients $(|F_O| - |F_C|)$ exp$\alpha_C \cdot \alpha_C$, calculated phase.

(6) Computer Time on a Siemens 4004/150 (Cycle Time 0.75 μsec)

Structure–factor calculation for 15,000 reflections and 1630 atoms	13,500 sec
Fourier synthesis 1.62 × 10^5 grid points	4000 sec
Real-space refinement for both chains in the asymmetric unit	17,000 sec

^{a} These values were used in model-building procedures 8 and 9 for probe length and filter constants. Also the variation of the angular value of τ was allowed, but not for Gly, Ser, and Thr. ^{b} After introduction of ω. ^{c} New value estimated with the data at 2.1-Å resolution. $^d\omega$ has been introduced after difference Fourier map 4 (data to 2.3-Å resolution, R factor value 0.29, B = 23 Å^2).

Experimental Procedure

The V$_{REI}$ dimer crystallizes in the space group $P6_1$. The hexagonal unit cell parameters are $a = b = 75.8$ Å, $c = 98.2$ Å, $\gamma = 120°$. The asymmetric unit contains one dimer molecule. Intensity data were collected to 2.0-Å resolution on a modified Siemens AED diffractometer using θ–2θ scan, with focus-to-crystal and crystal-to-detector distances of 30 cm each. The intensity profile of each reflection was scanned twice in steps of 1/100° (44 steps over the whole reflection). The counting time per step was set inversely proportional to the intensity at the peak of the reflection; the upper limit was set at 2.4 sec/step for reflections to a resolution of 2.5 Å. The reflections from 2.5- to 2.0-Å resolution were measured with 6 sec/step. Background was counted on both sides. The whole data set had been collected by diffractometers. The reflections were collected in shells of sin θ/λ. Film data obtained from screenless precession photographs which were evaluated using the method of Schwager et al. (Schwager et al., 1975) were included and used for scaling purposes. The data were corrected for absorption by an empirical method (Huber and Kopfmann, 1969). The complete intensity data set included 42,464 measurements (of which 5454 are film data), which were merged to 14,993 independent reflections (0.69 of the possible reflections to a resolution of 2.0 Å). All reflections to a resolution of 2.5 Å were used (10381), except the innermost reflections to a resolution of 6.8 Å (941) which are strongly influenced by the solvent continuum. To a resolution of 2.5 Å, 0.99 of the possible reflections is measured. From 2.5- to 2.0-Å resolution, only the reflections which could be observed above the 2σ significance level determined from counting statistics (3671) were used (e.g., 0.34 of the possible reflections in that range).

The neglect of the innermost reflections to a resolution of 6.8 Å does not influence Diamond's real-space refinement procedure. In the refinement of PTI (Deisenhofer and

Steigemann, 1975) the neglect of the innermost reflections improved the refinement of the positions of solvent molecules. We omitted these reflections from all calculations and did not consider them in the interpretation of the electron density map. The R value for all measurements, defined as

$$R = \left(\sum_h \sum_j^{N_h} (\langle I \rangle_h - I_{hj})^2 \Big/ \sum_h N_h \langle I \rangle_h{}^2 \right)^{1/2}$$

is 0.05 ($\langle I \rangle_h$ is the average intensity of the N_h measurements, I_{hj} are the individual measurements of a reflection h). The R_{sym} values for individual crystals lie between 0.022 and 0.065; the average R_{sym} is 0.04.

The crystal structure of REI has been refined by a constrained crystallographic refinement described in the refinement of the crystal structure of the bovine pancreatic trypsin inhibitor (PTI) (Deisenhofer and Steigemann, 1975) and in the refinement of the structure of the complex between bovine trypsin and PTI (Huber et al., 1974). This procedure involves cycles consisting of phase calculation using the current atomic model, Fourier synthesis using these calculated phases and the observed structure–factor amplitudes, and Diamond's real-space refinement (Diamond, 1971, 1974). At various stages (stagnation of further refinement), difference Fourier syntheses are calculated to detect and correct gross errors in the model (such as incorrect orientation of main-chain amides or side chains) and to localize solvent molecules. The stagnation of the refinement is reached, if the R factor value (definition see Table I) does not decrease further. Incorrectly oriented main-chain amides are rotated by reading the correct position of the carbonyl oxygen from the difference map and subjecting the whole chain to a model-building procedure (Diamond, 1966). Side-chain orientations are corrected by rotating around the appropriate dihedral angles. Some characteristics of the model-building procedure and the real-space refinement procedure are outlined in Table I. During the refinement 8 model-building procedures and 11 difference Fourier syntheses were calculated. The Fourier syntheses in the automatic cycles between these difference Fourier maps were mostly of the type $(2|F_o| - |F_c|) \exp \alpha_c$; a few $(3|F_o| - 2|F_c|) \exp \alpha_c$ were also used. Such syntheses increase the density gradients at the atomic positions and the speed of convergence. Table II shows the statistics of the course of the real-space refinement procedure.

Results and Discussion

Description of the Refinement. The starting model had been obtained through extensive real-space refinement of the model into the isomorphous Fourier map at 2.8-Å resolution. The above electron density map had first been averaged over the two independent molecules (Epp et al., 1974). The starting R factor (defined in Table I, 4) was 0.48. During the subsequent course of the refinement the two molecules in the asymmetric unit were refined independently. The coordinates of the second molecule were obtained by applying the known local symmetry. After several cycles the R factor decreased to a value of 0.39. At this stage, the first difference Fourier map was calculated. The coordinates were plotted onto the Fourier map to check the progress. Misplaced side chains and several incorrectly oriented main-chain amides were detected (Table II). Between succeeding difference Fourier maps three to five automatic refinement cycles were performed, depending on the progress of the refinement. The refinement was started with reflec-

Table II: Specifications of Difference Fourier Maps.

Difference Map No.	R Value	Corrections in Each Map		Resolution (Å)	Overall Temp Fact. (Å²)	Atom Radius $\langle r \rangle$(Å)
		Side Chains Main-Chain Amides Chain 1	Side Chains Main-Chain Amides Chain 2			
1	0.390	10	7	2.5	28	1.55
2	0.350	4	6	2.4	25	1.55
3	0.304	3	2	2.4	23	1.55
		11 solvent molecules				
4	0.294	4	2	2.3	23	1.55
		26 solvent molecules				
5	0.282	4	3	2.3	23	1.55
		40 solvent molecules				
6	0.270	1	1	2.2	23	1.55
		39 solvent molecules introduction of cis-prolines (Pro-8, Pro-95)				
7	0.264	1	1	2.2	23	1.55
		42 solvent molecules				
8	0.250	1	1	2.2	23	1.55
		36 solvent molecules				
9	0.241			2.1	23	1.55
		41 solvent molecules				
10	0.241			2.1	23	1.50
		55 solvent molecules				
11	0.241			2.0	21	1.50
		53 solvent molecules				

tion data to 2.5-Å resolution. During the course of the refinement further data were included to 2.0-Å resolution. An overall temperature factor was used, which was recalculated several times by comparing $|F_o|$ and $|F_c|$ and the temperature factor changed if necessary. An average atomic radius of 1.55 Å was used for all atoms throughout the refinement until difference Fourier map 9. Afterwards a new value of 1.50 Å was estimated by a trial calculation of atomic radii refinement in the real-space refinement step. This value is directly related to and consistent with the observed overall temperature factor of 21 Å². By the inspection of the difference Fourier maps, solvent molecules were detected and used in the phase calculations. The course of the difference maps is shown in Table II. The starting model had to be corrected in several segments. A number of main-chain amides and side chains had to be rotated. For the correction of main-chain amides, the presence of two identical molecules in the asymmetric unit provided a very useful cross-check. In difference Fourier map 6, the segments around Pro-8 and Pro-95 could be corrected. The local distribution of maxima and minima in these two regions was very similar and consistent in the two independent molecules, and it suggested the presence of cis-peptide groups (Huber and Steigemann, 1974). After the introduction of these *cis*-prolines, the refinement proceeded and stopped finally at an R factor value of 0.24. At this stage, 53 solvent molecules had been identified.

Description of the Electron Density Map. Figure 1a and b is stereo pictures of the electron density and the model fit at two amino acid residues (Gln-37 and Tyr-71)[1] in order to

[1] Amino acid residue numbers are those of the V_{REI} sequence. The nomenclature recommended by IUPAC–IUB (1970) is used in this paper with additional definitions as given by Diamond (1966, 1971, 1974). The coordinates of the V_{REI} dimer are available upon request. They are also in the Protein Data Bank of Brookhaven National Laboratory. Coordinates as well as stereo drawings are contained in R. Feldmann's Global Atlas of Protein Structure on Microfiche.

DOCKET ALARM

Explore Litigation Insights

Docket Alarm provides insights to develop a more informed litigation strategy and the peace of mind of knowing you're on top of things.

Real-Time Litigation Alerts

Keep your litigation team up-to-date with **real-time alerts** and advanced team management tools built for the enterprise, all while greatly reducing PACER spend.

Our comprehensive service means we can handle Federal, State, and Administrative courts across the country.

Advanced Docket Research

With over 230 million records, Docket Alarm's cloud-native docket research platform finds what other services can't. Coverage includes Federal, State, plus PTAB, TTAB, ITC and NLRB decisions, all in one place.

Identify arguments that have been successful in the past with full text, pinpoint searching. Link to case law cited within any court document via Fastcase.

Analytics At Your Fingertips

Learn what happened the last time a particular judge, opposing counsel or company faced cases similar to yours.

Advanced out-of-the-box PTAB and TTAB analytics are always at your fingertips.

API

Docket Alarm offers a powerful API (application programming interface) to developers that want to integrate case filings into their apps.

LAW FIRMS

Build custom dashboards for your attorneys and clients with live data direct from the court.

Automate many repetitive legal tasks like conflict checks, document management, and marketing.

FINANCIAL INSTITUTIONS

Litigation and bankruptcy checks for companies and debtors.

E-DISCOVERY AND LEGAL VENDORS

Sync your system to PACER to automate legal marketing.

fastcase®
Smarter legal research.